JMEPEG (2012) 21:62–68
DOI: 10.1007/s11665-010-9823-x

1059-9495/$19.00

Measurement of In-Plane Shear Strength of Carbon/Carbon Composites by Compression of Double-Notched Specimens

K.F. Yan, C.Y. Zhang, S.R. Qiao, C.Z. Song, D. Han, and M. Li

(Submitted November 23, 2009; in revised form July 10, 2010)

The compression of a double-notched specimen was used to determine the in-plane shear strength (IPSS) of a carbon/carbon composite in the paper. The effects of the notch distance (*L*), thickness (*T*), and notch width (*W*) and supporting jig on the IPSS of the double-notched specimens were investigated numerically and experimentally. The fracture surfaces were examined by a scanning electron microscope. It was found that the IPSS varied with *L*. Thin specimen yielded low strength. *W* has little effect on IPSS. The main failure modes include the matrix shear cracking, delamination, fracture and pullout of fibers or fiber bundles. Meanwhile, a supporting jig can provide lateral support and prevent buckling, therefore lead to the failure in a shear mode.

Keywords carbon/carbon composites, double-notched specimen, in-plane shear strength

1. Introduction

Carbon fiber-reinforced carbon matrix composite (C/C) exhibits superior thermo-mechanical properties at high temperatures, even above 2000 K. Therefore, it is expected to be used as high temperature structural components (Ref 1-3). Its physical and mechanical properties are directional. Therefore, the strength and failure behaviors of C/C depend on how the composite is loaded with respect to the principal material directions, in addition to the fiber/matrix and constituent properties. Shear deformation and failure might be dominant when the composite is loaded in off-axis directions or there are holes, notches and attachments in the structural component (Ref 4, 5). Such shear failure could take place either within the plane of composite, i.e. in-plane, or within the plane of thickness, i.e. interlaminar. The shear failure could lead to the disastrous results due to the low shear strength of C/C. Therefore, the shear deformation and failure behaviors must be studied to avoid and predict the unexpected failure in advance. For the in-plane shear, a common method to measure the in-plane shear strength (IPSS) of continuous fiber-reinforced ceramic matrix composite (including C/C) is the Iosipescu method, where a specimen in the form of a rectangular flat strip with two symmetric central V-notches is loaded using a mechanical testing machine and a four-point asymmetric fixture at room temperature (Ref 3, 4, 6, 7). However, the method cannot be used at elevated temperatures because the specimen cannot be tightly clamped due to the different thermal expansion coefficients between the specimen and jigs.

The compression of the double-notched specimen (DNS) had been used in determining the interlaminar strength of ceramic matrix composites at elevated temperatures (Ref 8). Failure of the specimen occurs between two central notches machined halfway through the thickness of the specimen and spaced a fixed distance apart on opposing faces. The advantages of this method for measuring IPSS at high temperatures include easy clamping at elevated temperatures and simple specimen configuration (Ref 9-13). Choi and Ünal, and so on, investigated the IPSS of some ceramic matrix composites at elevated temperatures by this method. Figure 1 shows a schematic figure of the DNS. Previous investigations indicate that the notch distance (*L*), notch width (*W*) and specimen supporting jig had great influences on the interlaminar shear strength of the ceramic matrix composites (Ref 9), whereas, the effects of such parameters on the IPSS had not been systematically studied.

Therefore, the IPSS of C/C was evaluated by loading in compression a DNS of uniform width in the paper. The effects of the *L*, *W*, and thickness (*T*) of the specimen, shown in Fig. 1, on the IPSS were investigated numerically and experimentally. Also, the effects of a supporting jig on the stress distribution and failure mode of C/C were also studied.

2. Finite Element Modeling (FEM) Analysis

The IPSS was determined by loading in compression of a DNS specimen. The dimensions of the DNS used were different from those specified in ASTM C1292-00 (Ref 6), ASTM C1425-05 (Ref 8) and ASTM D3846-02 (Ref 14), which were used to measure the interlaminar shear strength of ceramic matrix composites. Therefore, the stress distributions

K.F. Yan, C.Y. Zhang, S.R. Qiao, C.Z. Song, D. Han, and **M. Li**, National Key Laboratory of Thermostructure Composite Materials, Northwestern Polytechnical University, 547 Mailbox, 127 Youyi West Road, Xi'an 710072 Shaanxi, People's Republic of China. Contact e-mail: cyzhang@nwpu.edu.cn.

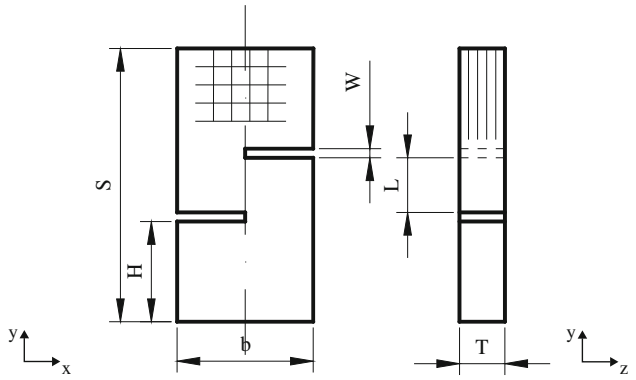

Fig. 1 Schematic figure of the double-notched specimen used to determine the IPSS

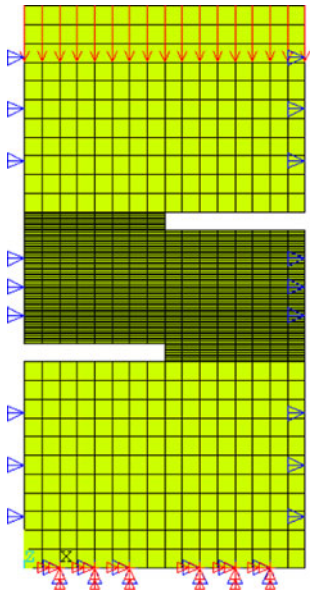

Fig. 2 The boundary conditions of the DNS used for the modeling

in the specimens were investigated first. The finite element model, consisting of 1380 elements and 5304 nodes, was applied. Attention was paid to the stress between the two notches. The parameters used in the model were as follows: $E_{11} = E_{22} = 32$ GPa, $E_{33} = 5.1$ GPa, $\nu_{13} = \nu_{23} = 0.2$, $\nu_{12} = 0.05$, $G_{13} = G_{23} = 1.1$ GPa, $G_{12} = 5.8$ GPa.

2.1 Boundary Conditions

A schematic diagram of the specimen and boundary conditions is shown in Fig. 2. One end of the specimen was fixed where no movement and rotation was allowed. A boundary conditions, in which the displacement in x-direction was fixed, was applied on the nodes in order to avoid the buckling effect. Other ends were subject to a uniform load of 50 N.

2.2 Effects of Various Parameters on the Stress Distribution

The distributions of the normalized transverse stress (σ_x), axial stress (σ_y) and shear stress (τ_{xy}) between the notches in the specimen are shown in Fig. 3. The normalization was fulfilled by dividing the average stresses at nodes between the notches. The total length, width (b) and T of the specimen are 30, 15 and 3 mm, respectively. L varied from 4 to 12 mm in a step of 2 mm. It can be seen that a similar trend was present for the distributions of the three kinds of stress. The distributions of the three kinds of stresses are not uniform in the specimens with the different L. Intense stress concentrations take place near the notch roots. However, the distributions of the three kinds of stress are different. σ_x is compressive in the vicinity of the notches and becomes tensile at the position close to the midsection of the specimen. σ_y is compressive between the notches. τ_{xy} is zero at the exact notch roots, followed by a abrupt jump to the maximum shear stress, then decreases rapidly to a nearly constant value at the midsection. The distributions of the stresses in the DNS are same as those of the interlaminar specimen (Ref 9, 11).

The plane between the notch roots is considered as the ideal fracture plane under shear loading. Therefore, more attention was paid to the distribution of τ_{xy}. The stress concentration factor K_t of τ_{xy} can be calculated by $K_t = \tau_{max}/\tau_{ave}$, where τ_{max} and τ_{ave} are maximum stress and average stress, respectively. The smaller the K_t is, the more uniform the distribution of τ_{xy} is. The K_t of the specimens with L of 4, 6, 8, 10 and 12 mm are 1.94, 2.26, 2.47, 2.64 and 2.80, respectively. The result means that the distribution of τ_{xy} between the notches is more uniform for the smaller L. It is caused by the interaction of the stress fields around the notches. The maximum shear stress (τ_{max}) can also be calculated as follows: $\tau_{max} = \tau\theta \coth \theta$ (Ref 15), where τ is the average stress, equal to P/LT, P is the load, $\theta = 2Lk/b$, $k = \sqrt{G_{xy}/2E_x}$, E_x is the elastic modulus and G_{xy} is the shear modulus. It can be found that the smaller L can lead to the smaller τ_{max}, indicating more uniform distribution of τ_{xy} between the notches.

Figure 4 shows the effects of the T on the distribution of τ_{xy}. Figure 5 presents the distributions of σ_x and τ_{xy} in the specimen with W of 1 and 2 mm. The total length, L and b are 30, 6 and 15 mm, respectively. The distributions of stresses are the same as the results in Fig. 3. It is obvious that the T and W have little affects on the distributions of τ_{xy}.

In order to allow for the uniform axial compression of the specimen, and to provide lateral support to prevent buckling, a supporting jig was used. The numerical analyses of the stress distribution were also carried out for the specimens with and without a supporting jig. The specimen dimensions modeled are $b = 15$, $L = 6$, $T = 3$ and $W = 1$ mm. Figure 6 illustrates the boundary conditions of the DNS with and without a supporting jig. The distributions of normalized σ_x and τ_{xy} with and without a supporting jig are shown in Fig. 7. It is found that the stress concentrations are greatly reduced by using a supporting jig. σ_x in the specimen is tensile if the specimen is not supported by a jig. However, it becomes compressive when the specimen is clamped by a supporting jig. The results indicate that a supporting jig can make the distribution of τ_{xy} more uniform.

3. Experimental

The C/C consists of polyacrylonitrile derived carbon fibers and pyrolytic carbon matrix. The preform was a 0°/90° continuous carbon fibers and sandwiched short carbon fiber felt. The carbon matrix was prepared by a chemical vapor

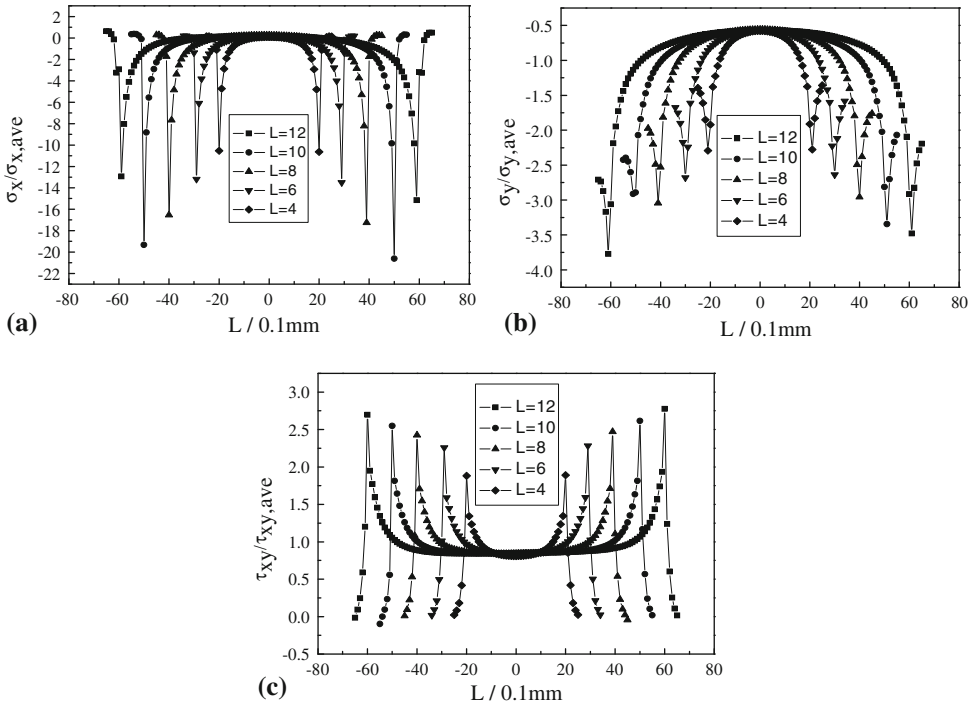

Fig. 3 Distributions of normalized stresses of C/C with various *L*. (a) σ_x, (b) σ_y and (c) τ_{xy}

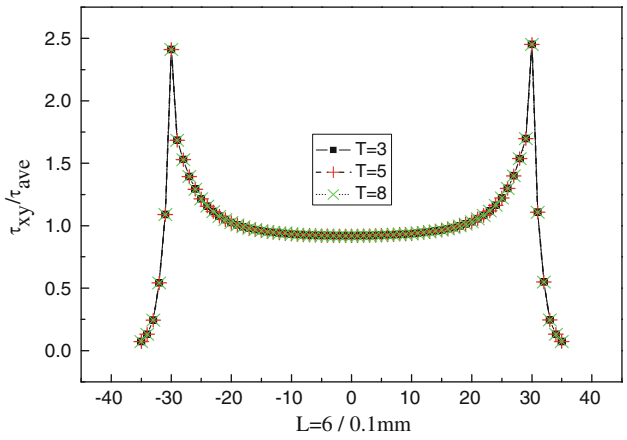

Fig. 4 Distribution of normalized τ_{xy} in the DNS with *T* of 3, 5, and 8 mm, respectively

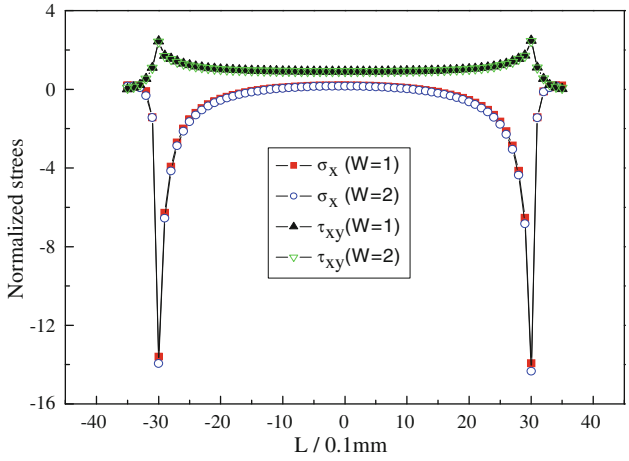

Fig. 5 Distribution of normalized σ_x and τ_{xy} in the specimens with $W = 1$ and 2 mm

infiltration technique. The density, residual porosity and overall fiber volume fraction are 1.50 kg/m^3, 17 and 25%, respectively. The specimens were cut into rectangular plates with two notches machined on both sides. The depth of the notches was at least equal to one half of the specimen thickness. The specimen shape is shown in Fig. 1 and the dimensions of the specimens are shown in Table 1. Seven specimens were prepared for each parameter. Also another 7 specimens were machined to investigate the effects of a supporting jig on the IPSS.

The IPSS of C/C were measured by loading in compression a DNS of uniform width. The experiments were performed in a mechanical testing machine (CSS-280S-100) at room temperature. The cross-head speed was 0.5 mm/min. The fractured surfaces were observed by scanning electron microscope (SEM, HITACHI S-4700). The IPSS was calculated by the equation.

$$\text{IPSS} = \frac{P_{\max}}{LT} \qquad \text{(Eq 1)}$$

where $P_{\max}$ is the maximum load.

4. Results and Discussion

Figure 8 shows a typical load-crosshead displacement curve. It is found that the curve can be divided into three parts. The first part is nonlinear, which results from the self-aligning processes between the fixture and the specimen under

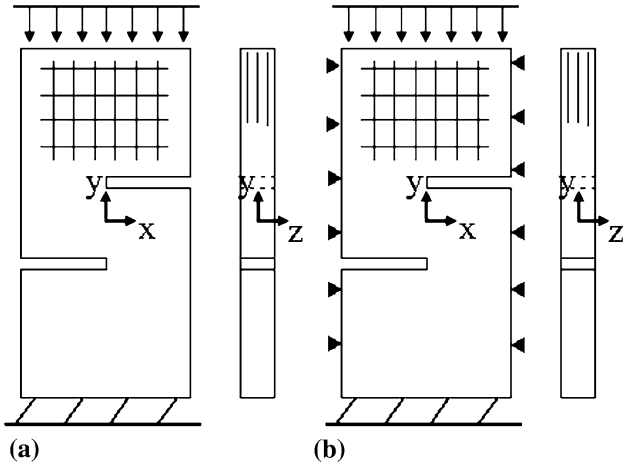

Fig. 6 The boundary condition of the DNS. (a) With a supporting jig and (b) without a supporting jig

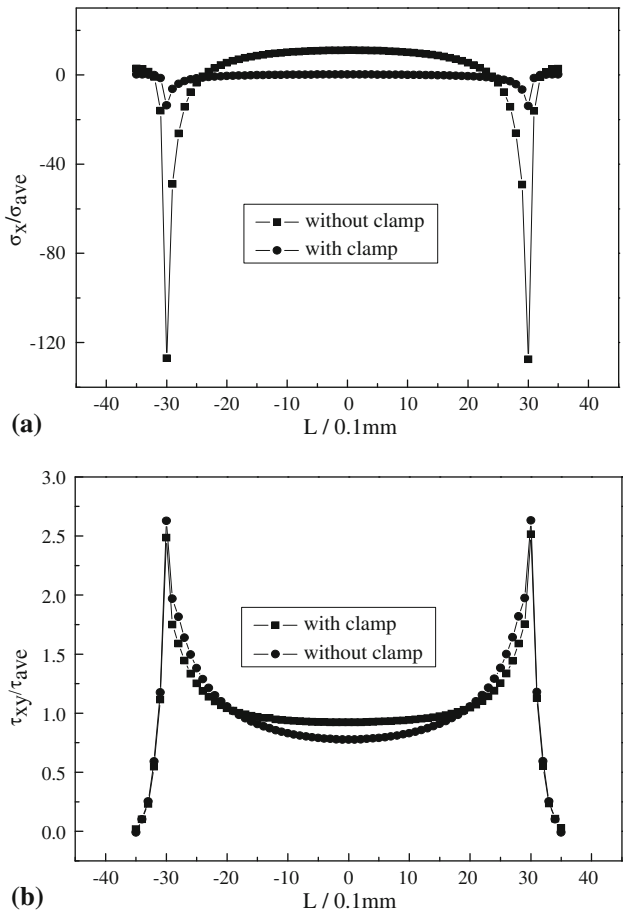

Fig. 7 Distributions of normalized stresses in the DNS with and without a supporting jig. (a) σ_x and (b) τ_{xy}

the initial loading. Followed the first part, a linear deformation process can be seen. The linear deformation process can be explained by the rule of mixture, that is, the loads shared by the carbon and matrix are proportional to their volume fraction. The result is similar to that on C/SiC (Ref 16). The third part is also a nonlinear process. It is caused by the accumulation of the

Table 1 Dimension of various in-plane shear specimens

Specimen	*L*, mm	*H*, mm	*T*, mm
A	4	12	3
B	6	11	3
C	8	10	3
D	6	11	5
E	6	11	8
F	6	11	3

The total length of specimen and *b* is 30 and 15 mm, respectively. For specimen A-E, *W* is 1 mm. For specimen F, *W* is 2 mm

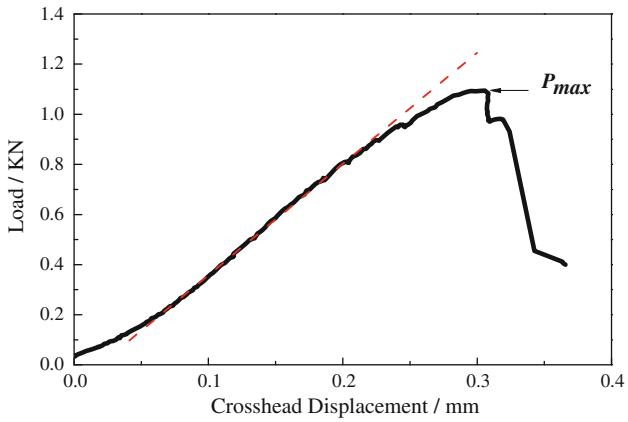

Fig. 8 A typical load-displacement curve when the DNS was loaded in compression at the crosshead rate of 0.5 mm/min. The *L*, *T* and *W* of specimens are 6, 3, and 1 mm, respectively

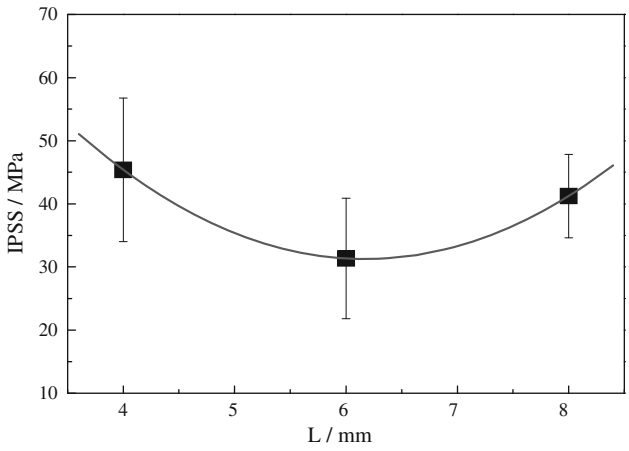

Fig. 9 The IPSS of C/C determined by compression of the DNS with *L* of 4, 6, and 8 mm, respectively

matrix cracks and interfacial friction between the matrix and fibers (Ref 4, 7).

The values of the IPSS of the DNS with different *L* are shown in Fig. 9. Obviously, that the magnitude of *L* has significant influences on the IPSS. The smallest IPSS can be obtained for the samples with *L* of 6 mm. According to the stress distribution in Fig. 3, the smaller *L* can lead to more uniform distribution of the stresses and lower extent of stress concentration around the notch roots. As a result, the IPSS of

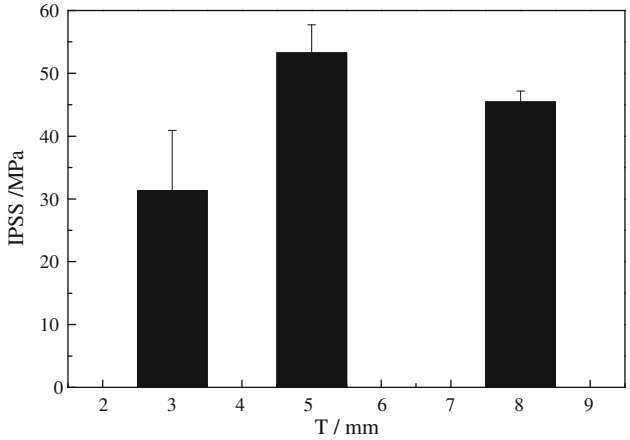

Fig. 10 The IPSS of C/C measured by using the DNS specimen with T = 3, 5, and 8 mm, respectively

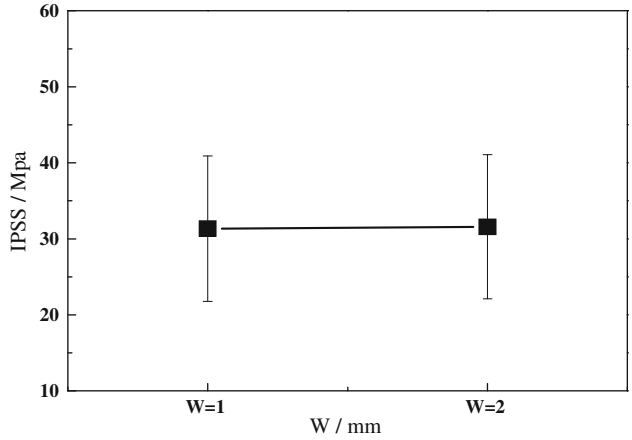

Fig. 11 The IPSS of the DNS with W of 1 and 2 mm

the DNS with L = 4 is larger than that with L = 6. For the DNS with L of 8 mm, the friction between the specimen and the supporting jig plays an important role in determining the IPSS of the DNS with larger L (Ref 17), although the extent of stress concentrate increases around the notch roots. More loads were needed to overcome the friction force for the DNS with larger L. So the IPSS of the DNS with L = 8 is larger than that with L = 6. The trend is the similar to that for the interlaminar shear strength of ceramic matrix composites (Ref 18). Actually, it is reasonable to choose the minimum value of the IPSS in using and designing the materials. Therefore, the DNS with L of 6 mm should be applied in measuring the IPSS of C/C.

The effects of T on the IPSS of C/C can be found in Fig. 10. The IPSS of the DNS with T = 3 mm is the smallest among the three kinds of the specimens, even although the same stress distributions in the specimens with different T, indicated in Fig. 4. According to the local load-sharing theory, the load previously carried by the broken fibers can not be undertaken equally by the surviving fibers located on the same plane. A stress concentration appears at the intact fibers located near the broken fibers. For the thinner specimens, the stress concentrations become greater and the composites can fail at lower stresses. Moreover, the damage zone produced by the same machining process should be the same for all specimens. The proportion of the damaged zone, defined by the surface area divided by the specimen volume (Ref 19), is larger in the thinner specimens than that in the thicker specimens. Therefore, the strength of the DNS with T of 3 mm is smaller than that of the thicker specimens. The IPSS decreases when the thickness changes from 5 to 8 mm. It can be explained by the size effect, which means that more flaws survive in the thicker specimens.

Figure 11 presents the IPSS of the DNS with W of 1 and 2 mm. It can be found that the magnitudes of IPSS are almost same for both kinds of the specimens. This result is the same as the result in other's work (Ref 11).

The DNS failed in a plane perpendicular to the compressive loading when the specimen was not supported by a jig, shown in Fig. 12(a). It is caused by the buckling effect. The stress perpendicular to the loading direction exceeded the ultimate strength of C/C before the shear stress reach the IPSS. Figure 12(b) shows the failure mode of the DNS when the specimens were clamped by a supporting jig. Failure of the specimen occurs by shear between two centrally located

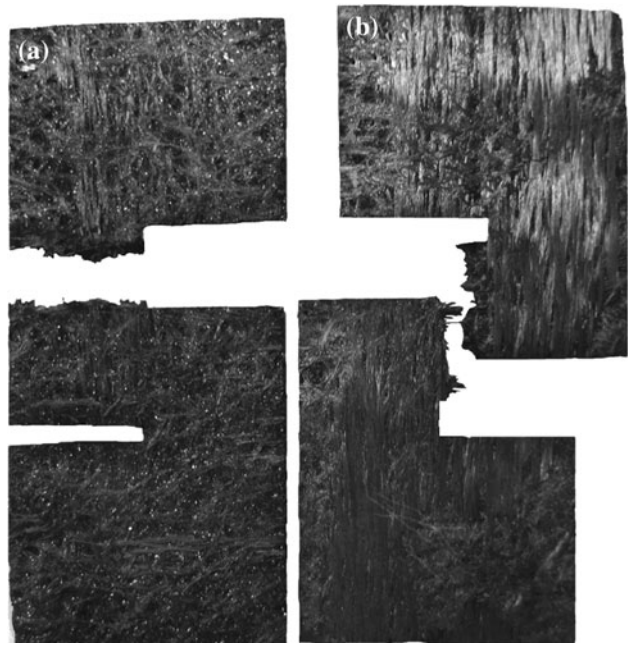

Fig. 12 A macroscopic view of the DNS supported without and with a jig. The applied crosshead rates are 0.5 mm/min

notches. The fractured plane is desirable in shear stress. According to the numerical results in Fig. 6, σ_x, which is responsible for the crack prorogation along the plane perpendicular to the compressive loading, was tensile when the specimen was supported by a jig, whereas it became compressive stress for the specimen without a supporting jig. In order to obtain the effective IPSS, a supporting jig must be applied.

Figure 13(a) shows a SEM photograph taken on a fracture surface. The different failure modes can be found on the plane. The debonding took place for the fiber/matrix interface, where the fibers were parallel to the loading direction, as shown in Fig. 13(b). The τ_{max} always located around the notch roots. So the cracks preferred to be formed here. Because the interface strength is lower than the strength of matrix and fibers, the crack can easily grow along the interface where the fibers are parallel to the loading direction. The fibers perpendicular to the loading direction were pulled out from the fracture plane, as

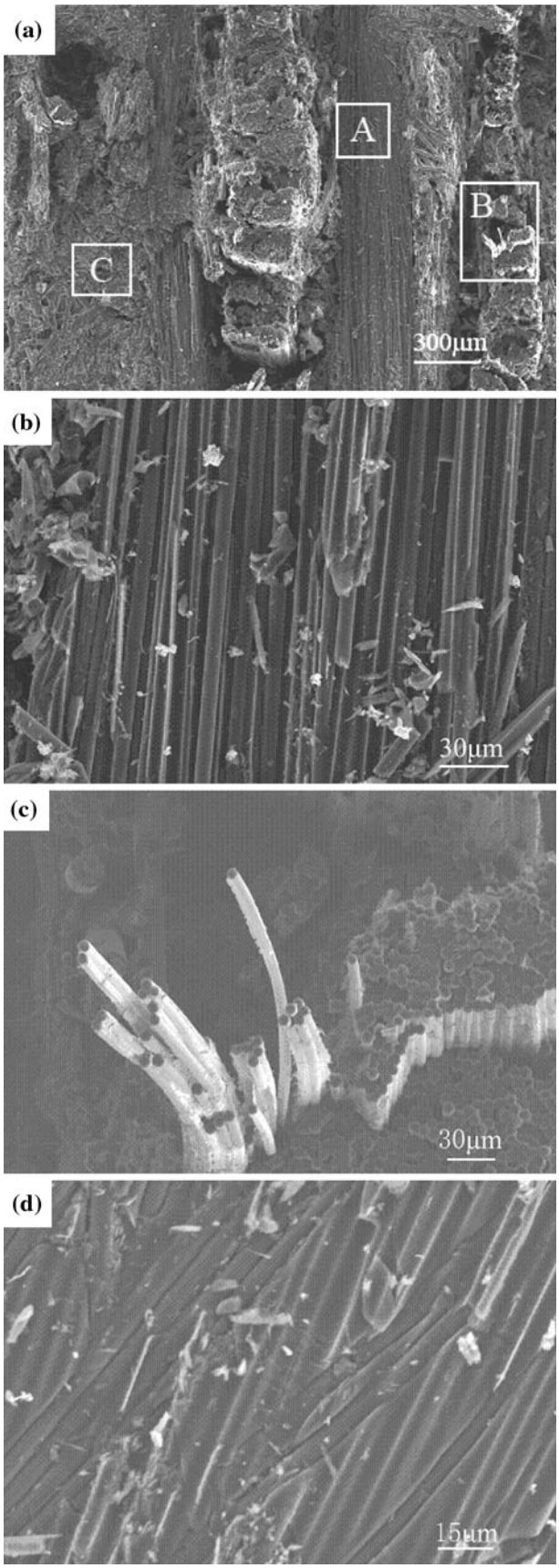

Fig. 13 SEM images taken on the fracture surfaces of C/Cs, (b), (c) and (d) are the magnified pictures of zone A, B and C in (a), respectively

shown in Fig. 13(c). When the cracks passed the perpendicular fibers, the fibers broke and were pulled out. In addition, the carbon matrix cracked under the shear stress, as indicated in Fig. 13(d).

5. Conclusions

(1) The distribution of the shear stress between the notch roots of the DNS is not uniform. There are intense concentrations around the notch roots. The distribution of the stress becomes more uniform for the DNS with smaller L.

(2) A supporting jig could reduce the stress concentrations significantly between the notches. The failure in the shear manner was achieved by using a supporting jig.

(3) Compression of the DNS is an effective method to measure the IPSS of C/C. The specimen consists of a rectangular plate of 30 mm × 15 mm × 3 mm. The recommended values of the L, T and W are 6, 3, and 1 mm, respectively.

Acknowledgments

The authors would like to acknowledge the financial support from National Science Foundation of China (Grant No. 50702045), Ph.D. Programs Foundation of Ministry of Education of China (Grant No. 20070699007) and the Program for New Century Excellent Talents in University (NCET-08-0460).

References

1. H. Hatta, K. Goto, and T. Aoki, Strengths of C/C Composites Under Tensile, Shear, and Compressive Loading: Role of Interfacial Shear Strength, *Compos. Sci. Technol.*, 2005, **65**, p 2550–2562
2. M.V. Rao, P. Mahajan, and R.K. Mittal, Effect of Architecture on Mechanical Properties of Carbon/Carbon Composites, *Compos. Struct.*, 2008, **83**(2), p 131–142
3. L.R. Bradley, C.R. Bowen, B. McEnaney, and D.C. Johnson, Shear Properties of a Carbon/Carbon Composite with Non-Woven Felt and Continuous Fiber Reinforcement Layers, *Carbon*, 2007, **45**, p 2178–2187
4. P. Brondsted, F.E. Heredia, and A.G. Evans, In-Plane Shear Properties of 2-D Ceramic Matrix Composites, *J. Am. Ceram. Soc.*, 1994, **77**(10), p 2569–2574
5. U.A. Khashaba, In-Plane Shear Properties of Cross-Ply Composite Laminates with Different Off-Axis Angles, *Compos. Struct.*, 2004, **65**(2), p 167–177
6. ASTM C-1292-00, *Standard Test Method for Shear Strength of Continuous Fiber-Reinforced Advanced Ceramics at Ambient Temperatures*, ASTM Designation, 2005
7. L. Denka, H. Hatta, A. Misawa, and S. Somiya, Shear Fracture of C/Cs Composites with Variable Stacking Sequence, *Carbon*, 2001, **39**(10), p 1505–1513
8. ASTM C-1425-05, *Standard Test Method for Interlaminar Shear Strength of 1-D and 2-D Continuous Fiber-Reinforced Advanced Ceramics at Elevated Temperatures*, ASTM Designation, 2005
9. J.J.F. Nancy and T.W. Chou, Characterization of Interlaminar Shear Strength of Ceramic Matrix Composites, *J. Am. Ceram. Soc.*, 1993, **76**(10), p 2539–2548
10. M.M. Shokrieh and L.B. Lessard, An Assessment of the Double-Notch Shear Test for Interlaminar Shear Characterization of a Unidirectional Graphite/Epoxy Under Static and Fatigue Loading, *Appl. Compos. Mater.*, 1998, **5**, p 289–304
11. P. Dadras and J.S. Mcdowell, Analytical and Experimental Evaluations of Double-Notch Shear Specimens of Orthotropic Materials, *Exp. Mech.*, 1990, **30**(2), p 184–189

12. Ö. Ünal and N.P. Bansal, In-Plane and Interlaminar Shear Strength of a Unidirectional Hi-Nicalon Fiber-Reinforced Celsian Matrix Composite, *Ceram. Int.*, 2002, **28**(5), p 527–540
13. S.R. Choi and N.P. Bansal, Shear Strength as a Function of Test Rate for SiC_f/BSAS Ceramic Matrix Composite at Elevated Temperature, *J. Am. Ceram. Soc.*, 2004, **87**(10), p 1912–1918
14. ASTM D-3846-02, *Standard Test Method for In-Plane Shear Strength of Reinforced Plastics*, ASTM Designation, 2001
15. M.F. Markham and D. Dawson, Interlaminar Shear Strength of Fiber-Reinforced Composites, *Composites*, 1975, **6**(4), p 173–176
16. L. Hana and F. Ansorge, Damage and Failure Behaviour of a Woven C/SiC Material, *J. Mater. Sci.*, 1997, **32**, p 5467–5475
17. E.L. Curzio, D. Bowers, and M.K. Ferber, The Interlaminar Tensile and Shear Behavior of a Unidirectional C/C Composite, *J. Nucl. Mater.*, 1996, **230**, p 226–232
18. E.L. Curzio and M.K. Ferber, Shear Strength of Continuous Fiber Ceramic Composites, *Thermal and Mechanical Test Methods and Behavior of Continuous Fiber Ceramic Composites*, ASTM STP 1309, 1996, p 31–49
19. T. Nozawa, T. Hinoki, and Y. Katoh, Specimen Size Effects on Tensile Properties of 2D/3D SiC/SiC Composites, *Small Specimen Test Techniques*, ASTM STP 1418, 2002, p 294–305